Hydromagnetic flow in a viscoelastic fluid due to the oscillatory stretching surface

Z. Abbas, Y. Wang, T. Hayat, M. Oberlack

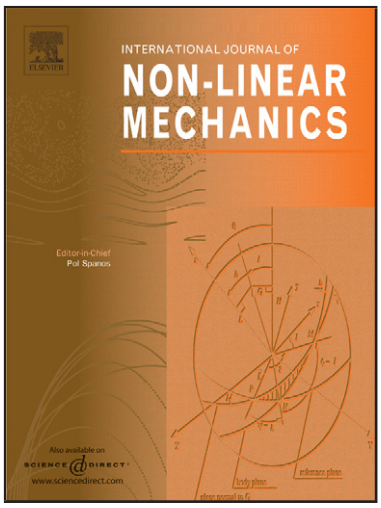

Hydromagnetic flow in a viscoelastic fluid due to the oscillatory stretching surface

Z. Abbas, Y. Wang, T. Hayat, M. Oberlack

PII: S0020-7462(08)00073-5
DOI: doi:10.1016/j.ijnonlinmec.2008.04.009
Reference: NLM 1475

To appear in: *International Journal of Non-Linear Mechanics*

Received date: 1 December 2007
Revised date: 13 April 2008
Accepted date: 15 April 2008

Cite this article as: Z. Abbas, Y. Wang, T. Hayat and M. Oberlack, Hydromagnetic flow in a viscoelastic fluid due to the oscillatory stretching surface, *International Journal of Non-Linear Mechanics*, doi:10.1016/j.ijnonlinmec.2008.04.009

Hydromagnetic flow in a viscoelastic fluid due to the oscillatory stretching surface

Z. Abbas[a,b,1], Y. Wang[a], T. Hayat[c] and M. Oberlack[a]

[a]Chair of Fluid Dynamics, Department of Mechanical Engineering, Darmstadt University of Technology, Darmstadt 64289, Germany

[b]Department of Mathematics, Faculty of Basic and Applied Sciences, IIU, Islamabad 44000, Pakistan

[c]Department of Mathematics, Quaid-I-Azam University 45320, Islamabad 44000, Pakistan

Abstract: An analysis is carried out to study the unsteady magnetohydrodynamic (MHD) two-dimensional boundary layer flow of a second grade viscoelastic fluid over an oscillatory stretching surface. The flow is induced due to an infinite elastic sheet which is stretched back and forth in its own plane. For the investigated problem, the governing equations are reduced to a non-linear partial differential equation by means of similarity transformations. This equation is solved both by a newly developed analytic technique, namely homotopy analysis method (HAM) and by a numerical method employing the finite difference scheme, in which a coordinate transformation is employed to transform the semi-infinite physical space to a bounded computational domain. The results obtained by means of both methods are then compared and show an excellent agreement. The effects of various parameters like visco-elastic parameter, the Hartman number and the relative frequency amplitude of the oscillatory sheet to the stretching rate on the velocity field are graphically illustrated and analyzed. The values of wall shear stress for these parameters are also tabulated and discussed.

Keywords: Visco-elastic fluid, electrically conducting fluid, oscillatory stretching sheet, HAM solution, numerical solution.

1 Introduction

Many fluids such as blood, dyes, yoghurt, ketchup, shampoo, paint, mud, clay coatings, polymer melts, certain oils and greases etc. have complicated relations between stresses and strains. Such fluids do not obey the Newton's law of viscosity and are usually called non-Newtonian fluids. The flows of such fluids occur in a wide range of practical applications and have key importance in polymer devolatisation, bubble columns, fermentation, composite processing, boiling, plastic foam processing, bubble absorption and many others. Therefore, non-Newtonian fluids have attracted the attention of a large variety of researchers including the interests of experimentalists and theoreticians like engineers, modelers, physicists, computer scientists and mathematicians. However, as these fluids are in themselves varied in nature, the constitutive equations which govern them are many taking account of the variations of rheological properties. The model and hence, the arising equations, are much

[1]Corresponding author at: Department of Mathematics, Faculty of Basic and Applied Sciences, IIU, Islamabad 44000, Pakistan Tel.: +92 51 9019502 and Fax: +92-51-2601171. E-mail address: za_qau@yahoo.com (Z. Abbas)

more complicated and of higher order than the well known Navier-Stokes equations. The adherence boundary conditions are insufficient for the determinacy of unique solution. This issue has been discussed in the excellent and fundamental studies $[1-5]$. Now the literature on the non-Newtonian fluids is extensive. Some recent contributions in this direction are made in the investigations $[6-16$ and several refs. therein$]$. Furthermore, the boundary layer flow caused by a moving continuous solid surface occurs in several engineering processes. Specifically such flows encounter in aerodynamic extrusion of plastic sheets, wire drawing, glass fiber and paper production, cooling of an infinite metallic plate and polymer processing [17]. Sakiadis [18] attempted the first problem regarding boundary layer viscous flow over a moving surface having constant velocity. Later this problem has been studied extensively through various aspects. Very recent investigations relevant to this problem have been made in the $[19-23]$.

To the best of our information only Wang [24] discussed the viscous flow due to an oscillatory stretching surface. Although oscillatory stretching sheet induces the present flow but we also have a free stream velocity oscillating in time about a constant mean oscillatory flow [25, 26]. Despite recent advances in non-Newtonian fluids, it is still of interest to develop stretching flows involving non-Newtonian fluids. For example, no investigation is available in the literature which deals with the oscillatory stretching flow of non-Newtonian fluids. Therefore, in the present study we provide first such attempt for a second grade fluid (a subclass of viscoelastic fluids). The contribution is divided into six sections. In section two, mathematical formulation is developed. Section three contains the analytic solution of the non-linear problem employing the homotopy analysis method [27, 28]. The homotopy analysis method is a powerful technique that has been successfully applied to various non-linear problems $[29-44]$. Numerical solution is presented in section four. Results and discussion are given in section five. Section six synthesises the concluding remarks.

2 Flow analysis

We consider the unsteady two-dimensional magnetohydrodynamic (MHD) laminar flow of an incompressible viscoelastic fluid (obeying second grade model) over an oscillatory stretching sheet coinciding with the plane $\bar{y}=0$, the flow being confined to the semi-infinite space $\bar{y}>0$. The elastic sheet is stretched back and forth periodically with velocity $u_w = b\bar{x}\sin\omega t$ (b is the maximum stretching rate, $\bar{x}$ is the coordinate along the sheet and ω is the frequency) parallel to the $\bar{x}$-axis, as shown in Fig. 1. A constant magnetic field of strength B_0 is applied perpendicular to the stretching surface and the effect of the induced magnetic field is neglected, which is a valid assumption on a laboratory scale under the assumption of small magnetic Reynolds number. Under the usual boundary layer assumptions and in the absence of pressure gradient, the unsteady basic boundary layer equations governing the MHD flow of viscoelastic fluid are:

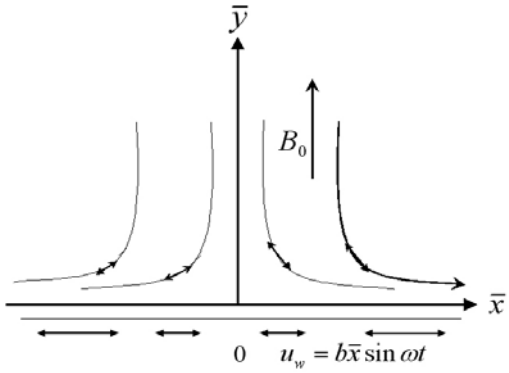

Fig. 1. Geometry of the problem

$$\frac{\partial u}{\partial \bar{x}} + \frac{\partial v}{\partial \bar{y}} = 0, \tag{1}$$

$$\frac{\partial u}{\partial t} + u\frac{\partial u}{\partial \bar{x}} + v\frac{\partial u}{\partial \bar{y}} = \nu\frac{\partial^2 u}{\partial \bar{y}^2} + \frac{k_0}{\rho}\left[\frac{\partial^3 u}{\partial t \partial \bar{y}^2} + \frac{\partial}{\partial \bar{x}}\left(u\frac{\partial^2 u}{\partial \bar{y}^2}\right) + \frac{\partial u}{\partial \bar{y}}\frac{\partial^2 v}{\partial \bar{y}^2} + v\frac{\partial^3 u}{\partial \bar{y}^3}\right] - \frac{\sigma B_0^2}{\rho}u. \tag{2}$$

In the above equations (u, v) are the velocity components in $(\bar{x}, \bar{y})$ directions respectively, ν is the kinematic viscosity of fluid, ρ is the fluid density, σ is the electrical conductivity of the fluid and k_0 is the visco-elastic parameter of the fluid

The appropriate boundary conditions of the problem are

$$u = u_w = b\bar{x}\sin\omega t, \quad v = 0 \quad \text{at} \quad \bar{y} = 0, \quad t > 0, \tag{3}$$

$$u = 0, \quad \frac{\partial u}{\partial \bar{y}} = 0 \qquad \text{as} \qquad \bar{y} \to \infty, \tag{4}$$

in which both b and ω have the dimension $(\text{time})^{-1}$. The second condition in (4) is the augmented condition since the flow is in an unbounded domain, which has been discussed by Garg and Rajagopal [45].

We assume

$$S \equiv \frac{\omega}{b}. \tag{5}$$

which denotes the ratio of the oscillation frequency of the sheet to its stretching rate.

Any particle path on the sheet is

$$\bar{x} = \bar{x}_0 \exp\left(\frac{1}{S}\cos\omega t\right). \tag{6}$$

The boundary conditions (3) and (4) suggest the following similarity transformations

$$y = \sqrt{\frac{b}{\nu}}\bar{y}, \qquad \tau = t\omega, \qquad u = b\bar{x}f_y(y,\tau), \qquad v = -\sqrt{\nu b}f(y,\tau). \tag{7}$$

Using the transformations (7), the continuity equation (1) is satisfied automatically and the governing equation (2) becomes

$$Sf_{y\tau} + f_y^2 - ff_{yy} + M^2 f_y = f_{yyy} + K\left(Sf_{yyy\tau} + 2f_y f_{yyy} - f_{yy}^2 - ff_{yyyy}\right), \tag{8}$$

and the boundary conditions (3) and (4) are reduced to

$$f_y(0,\tau)=\sin\tau,\qquad f(0,\tau)=0,\qquad f_y(\infty,\tau)=0\quad\text{and}\quad f_{yy}(\infty,\tau)=0, \tag{9}$$

in which $M^2=\sigma B_0^2/b\rho$ is the Hartmann number or the magnetic parameter and $K=bk_0/\nu\rho$ is the non-dimensional visco-elastic parameter. Here $K=0$ corresponds to the case of a Newtonian fluid.

A physical quantity of interest is the skin-friction coefficient C_f, which is defined as

$$C_f=\frac{\tau_w}{\rho u_w^2}, \tag{10}$$

where τ_w is wall skin friction, which is given by

$$\tau_w=\mu\left(\frac{\partial u}{\partial\bar{y}}\right)_{\bar{y}=0}+k_0\left(\frac{\partial^2 u}{\partial t\partial\bar{y}}+u\frac{\partial^2 u}{\partial\bar{x}\partial\bar{y}}+v\frac{\partial^2 u}{\partial\bar{y}^2}-2\frac{\partial u}{\partial\bar{y}}\frac{\partial v}{\partial\bar{y}}\right)_{\bar{y}=0}. \tag{11}$$

Using the variables (7), we get

$$\mathrm{Re}_x^{1/2}C_f=\left[f_{yy}+K\left(3f_yf_{yy}+Sf_{yy\tau}-ff_{yyy}\right)\right]_{y=0}, \tag{12}$$

where $\mathrm{Re}_x=u_w\bar{x}/\nu$ is the local Reynolds number.

3 Homotopy analysis method

Liao [27] proposed a new approximate analytical solution technique, called the Homotopy Analysis Method (HAM), for non-linear problems, which can overcome the foregoing restrictions of perturbation techniques. Different from perturbation methods, the validity of the HAM is independent on whether there exist small/large parameters in considered non-linear problems.

3.1 Homotopy analytic solution

In this part, we solve Eqs. (8) and (9) by means of homotopy analysis method (HAM). According to the boundary conditions (9) the velocity distribution $f(y,\tau)$ can be expressed by the set of base functions

$$\left\{y^k\sin(j\tau)\exp(-ny)\,\middle|\,k\geq 0,j\geq 0,n\geq 0\right\}$$

in the following form

$$f(y,\tau)=a_{0,0}^0+\sum_{n=0}^{\infty}\sum_{k=0}^{\infty}\sum_{j=0}^{\infty}a_{n,k}^j y^k\sin(j\tau)\exp(-ny), \tag{13}$$

in which $a_{n,k}^j$ are the coefficients. These provide us with the so-called *Rule of solution expressions* (see Liao [27]). With the help of these solution expressions and Eq. (9), it is straightforward to choose the initial approximations $f_0(y,\tau)$ for $f(y,\tau)$ as

$$f_0(y,\tau)=\sin\tau\left(1-\exp(-y)\right), \tag{14}$$

and the linear operator

$$\mathcal{L}_f\left(f\right)=\frac{\partial^3 f}{\partial y^3}-\frac{\partial f}{\partial y}, \tag{15}$$

which satisfies the following properties

$$\mathcal{L}_f\left[C_1+C_2\exp(-y)+C_3\exp(y)\right]=0, \tag{16}$$

where C_i $(i=1,2,3)$ are arbitrary constants.

Then, let $p\in[0,1]$ denotes an embedding parameter and $\hbar_f$ is a non-zero auxiliary parameter. We construct the zeroth-order deformation equation as

$$\left(1-p\right)\mathcal{L}_f\left[\widehat{f}\left(y,\tau;p\right)-f_0\left(y,\tau\right)\right]=p\hbar_f\mathcal{N}_f\left[\widehat{f}\left(y,\tau;p\right)\right], \tag{17}$$

subject to the boundary conditions

$$\begin{aligned}
\widehat{f}\left(0,\tau;p\right) &= 0, \qquad & \left.\frac{\partial\widehat{f}\left(y,\tau;p\right)}{\partial y}\right|_{y=0} &= \sin\tau,\\
\left.\frac{\partial\widehat{f}\left(y,\tau;p\right)}{\partial y}\right|_{y=\infty} &= 0, \qquad & \left.\frac{\partial^2\widehat{f}\left(y,\tau;p\right)}{\partial y^2}\right|_{y=\infty} &= 0,
\end{aligned} \tag{18}$$

and the non-linear operator $\mathcal{N}_f$ is defined as:

$$\begin{aligned}
\mathcal{N}_f\left[\widehat{f}\left(y,\tau;p\right)\right] = {} & \frac{\partial^3\widehat{f}\left(y,\tau;p\right)}{\partial y^3}-S\frac{\partial^2\widehat{f}\left(y,\tau;p\right)}{\partial y\partial\tau}+\widehat{f}\left(y,\tau;p\right)\frac{\partial^2\widehat{f}\left(y,\tau;p\right)}{\partial y^2}-\left(\frac{\partial\widehat{f}\left(y,\tau;p\right)}{\partial y}\right)^2\\
& -M^2\frac{\partial\widehat{f}\left(y,\tau;p\right)}{\partial y}+K\left\{\begin{array}{c} S\frac{\partial^4\widehat{f}(y,\tau;p)}{\partial^3 y\partial\tau}+2\frac{\partial\widehat{f}(y,\tau;p)}{\partial y}\frac{\partial^3\widehat{f}(y,\tau;p)}{\partial y^3}\\ -\left(\frac{\partial^2\widehat{f}(y,\tau;p)}{\partial y^2}\right)^2-\widehat{f}\left(y,\tau;p\right)\frac{\partial^4\widehat{f}(y,\tau;p)}{\partial y^4}\end{array}\right\}.
\end{aligned} \tag{19}$$

When $p=0$ and $p=1$, the above zeroth-order deformation problem has the following solutions, respectively

$$\widehat{f}\left(y,\tau;0\right)=f_0\left(y,\tau\right) \qquad \text{and} \qquad \widehat{f}\left(y,\tau;1\right)=f\left(y,\tau\right). \tag{20}$$

Thus, as p increases from 0 to 1, $\widehat{f}\left(y,\tau;p\right)$ varies from $f_0\left(y,\tau\right)$ to the solution $f\left(y,\tau\right)$ of the original equation (8). By Taylor's theorem and the relations (20), one can write

$$\widehat{f}\left(y,\tau;p\right)=f_0\left(y,\tau\right)+\sum_{m=1}^{\infty}f_m\left(y,\tau\right)p^m, \tag{21}$$

where

$$f_m\left(y,\tau\right)=\frac{1}{m!}\left.\frac{\partial^m\widehat{f}\left(y,\tau;p\right)}{\partial p^m}\right|_{p=0}. \tag{22}$$

Substituting the expansion (21) into the differential equation (17) and the corresponding boundary conditions (18), and equating coefficient of equal powers of p lead to the boundary-value problems for $f_m\left(y,\tau\right)$ $(m=0,1,2.....)$. Note that Eq. (17) contains the auxiliary parameter $\hbar_f$. The convergence of the series given in Eq. (21) strongly depends upon

this parameter $\hbar_f$. Therefore $\hbar_f$ should be properly chosen so that the above series (21) is convergent at $p = 1$. Hence, using Eq. (20), we have the solution series

$$f(y,\tau) = f_0(y,\tau) + \sum_{m=1}^{\infty} f_m(y,\tau). \tag{23}$$

We differentiate the zeroth-order equation m times with respect to embedding parameter p, then setting $p = 0$, and finally dividing by $m!$, we have the following mth-order deformation equation ($m \geq 1$)

$$\mathcal{L}_f\left[f_m(y,\tau) - \chi_m f_{m-1}(y,\tau)\right] = \hbar_f \mathcal{R}_m^f(y,\tau), \tag{24}$$

with boundary equations

$$f_m(0,\tau;p) = 0, \qquad \left.\frac{\partial f_m(y,\tau;0)}{\partial y}\right|_{y=0} = \left.\frac{\partial f_m(y,\tau;0)}{\partial y}\right|_{y=\infty} = \left.\frac{\partial^2 f_m(y,\tau;0)}{\partial y^2}\right|_{y=\infty} = 0, \tag{25}$$

where

$$\begin{aligned}\mathcal{R}_m^f(y,\tau) &= \frac{\partial^3 f_{m-1}}{\partial y^3} - S\frac{\partial^2 f_{m-1}}{\partial y \partial \tau} - M^2\frac{\partial f_{m-1}}{\partial y} + \sum_{k=0}^{m-1}\left(f_{m-1-k}\frac{\partial^2 f_j}{\partial y^2} - \frac{\partial f_{m-1-k}}{\partial y}\frac{\partial f_j}{\partial y}\right) \\ &+KS\frac{\partial^4 f_{m-1}}{\partial y^3 \partial \tau} + K\sum_{k=0}^{m-1}\left[2\frac{\partial f_{m-1-k}}{\partial y}\frac{\partial^3 f_j}{\partial y^3} - \frac{\partial^2 f_{m-1-k}}{\partial y^2}\frac{\partial^2 f_j}{\partial y^2} - f_{m-1-k}\frac{\partial^4 f_j}{\partial y^4}\right],\end{aligned} \tag{26}$$

and

$$\chi_m = \begin{cases} 0, & m \leq 1, \\ 1, & m > 1. \end{cases} \tag{27}$$

Note that, we obtain a linear non-homogeneous system equation in the form of high-order deformation equation, which is easy to solve using MATHEMATICA or other softwares. The general solution of Eq. (24) with $f_m^\star(y,\tau)$ denoting the special solution can be written as

$$f_m(y,\xi) = f_m^\star(y,\xi) + C_1 + C_2\exp(-y) + C_3\exp(y), \tag{28}$$

where the integral constants C_1, C_2 and C_3 are determined by the boundary conditions (18) and given by

$$C_2 = \left.\frac{\partial f_m^\star(y,\xi)}{\partial y}\right|_{y=0}, \quad C_1 = -C_2 - f_m^\star(0,\xi), \qquad C_3 = 0. \tag{29}$$

3.2 Convergence of the HAM solution

Liao [27] proved that, as long as a solution series given by the homotopy analysis method converges, it must be one of the solutions. Therefore, it is important to ensure that the solution series are convergent. The solution series (23) contains the non-zero auxiliary parameter $\hbar_f$, which can be chosen properly by plotting the so-called $\hbar$-curves to ensure the convergence of the solution series and rate of approximation of the HAM solution, as proposed by Liao [27]. To find the admissible values of $\hbar_f$, $\hbar$-curves of $f''(0,0)$ are shown in Fig. 2 for 15th-order of approximation for two groups of different parameters values: $S = 0.2$, $M = 1$, $K = 0.3$ and $S = 0.5$, $M = 2$, $K = 0.5$, respectively. From this figure, it can be seen that $\hbar$-curve has a parallel line segment that corresponds to a region $-1.2 \leq \hbar_f \leq -0.2$ for $S = 0.2$,

$M = 1$, $K = 0.3$ and $-0.45 \leq \hbar_f \leq -0.1$ for $S = 0.5$, $M = 2$, $K = 0.5$, respectively. To assure the convergence of the HAM solution, the values of the $\hbar_f$ should be chosen from these regions. The region for the values of $\hbar_f$ is dependent on the values of involving parameters. We can see that for the different values of the parameters, we get different $\hbar$-curves (for the admissible values of $\hbar_f$). It is evident from our calculations that the solution series (23) converges in the whole region of y if it is convergent at $y = 0$ when the proper values of $\hbar_f$ is chosen. Table 1 shows the convergence of the HAM solutions $f''(0, \tau)$ for several different times ($\tau = 0, 0.5\pi, 0.75\pi, 1.5\pi$) at different orders of approximation when $S = 0.3$, $M = 1.2$ and $K = 0.2$. For different times τ different $\hbar$-values are chosen from the admissible ranges of the corresponding $\hbar$-curves. It is shown that with the increase of the order of approximation a convergent solution can be reached.

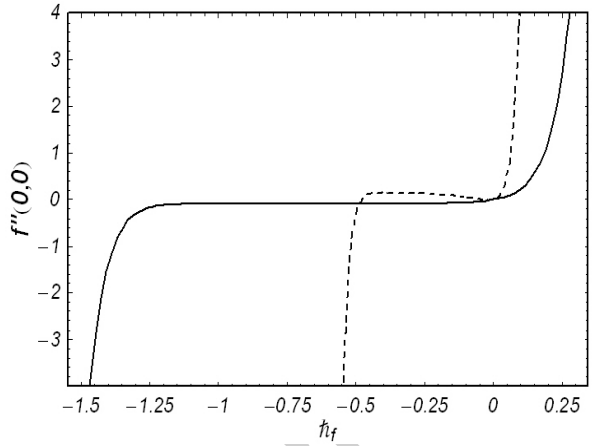

Fig. 2. The $\hbar$-curve of $f''(0, 0)$ at the 15th-order of approximation: Solid line with $S = 0.2$, $M = 1$ and $K = 0.3$ and Dashed line with $S = 0.5$, $M = 2$ and $K = 0.5$.

Order of approximations	$\tau = 0$ $\hbar_f = -0.7$	$\tau = 0.5\pi$ $\hbar_f = -0.5$	$\tau = 0.75\pi$ $\hbar_f = -0.4$	$\tau = 1.5\pi$ $\hbar_f = -0.45$
1	−0.08400	−1.31005	−0.82134	0.91913
3	−0.09735	−1.41491	−0.91400	0.83429
5	−0.10051	−1.42701	−0.93798	0.80239
10	−0.10197	−1.42876	−0.94599	0.78789
12	−0.10205	−1.42878	−0.94620	0.78716
15	−0.10209	−1.42878	−0.94627	0.78683
18	−0.10209	−1.42878	−0.94628	0.78679
20	−0.10209	−1.42878	−0.94628	0.78679
30	−0.10209	−1.42878	−0.94628	0.78679

Table 1. The convergence of the HAM solution of $f''(0, \tau)$ for different order of approximations with $S = 0.3$, $K = 0.2$, $M = 1.2$ and $\tau = 0, 0.5\pi, 0.75\pi$ and 1.5π, respectively.

4 Numerical method

The non-linear boundary-value problem (8) and (9) is also solved by means of the finite difference method. For this purpose, the coordinate transformation $\eta = 1/(y + 1)$ is applied

for transforming the semi-infinite physical domain $y \in [0, \infty]$ to a finite calculation domain $\eta \in [0, 1]$, i.e.,

$$y = \frac{1}{\eta} - 1, \qquad \frac{\partial}{\partial y} = -\eta^2 \frac{\partial}{\partial \eta}, \qquad \frac{\partial^2}{\partial y^2} = \eta^4 \frac{\partial^2}{\partial \eta^2} + 2\eta^3 \frac{\partial}{\partial \eta}, \qquad \frac{\partial^2}{\partial y \partial \tau} = -\eta^2 \frac{\partial^2}{\partial \eta \partial \tau},$$

$$\frac{\partial^3}{\partial y^3} = -\eta^6 \frac{\partial^3}{\partial \eta^3} - 6\eta^5 \frac{\partial^2}{\partial \eta^2} - 6\eta^4 \frac{\partial}{\partial \eta}, \qquad \frac{\partial^4}{\partial y^3 \partial \tau} = -\eta^6 \frac{\partial^4}{\partial \eta^3 \partial \tau} - 6\eta^5 \frac{\partial^3}{\partial \eta^2 \partial \tau} - 6\eta^4 \frac{\partial^2}{\partial \eta \partial \tau},$$

$$\frac{\partial^4}{\partial y^4} = \eta^8 \frac{\partial^4}{\partial \eta^4} + 12\eta^7 \frac{\partial^3}{\partial \eta^3} + 35\eta^6 \frac{\partial^2}{\partial \eta^2} + 24\eta^5 \frac{\partial}{\partial \eta}.$$

With these transformations, the differential equation (8) in terms of η can be rewritten in the forms

$$\begin{aligned} & S\left(1 - 6K\eta^2\right) \frac{\partial^2 f}{\partial \tau \partial \eta} - SK\eta^4 \frac{\partial^4 f}{\partial \eta^3 \partial \tau} - 6SK\eta^3 \frac{\partial^3 f}{\partial \eta^2 \partial \tau} \\ = \; & \left(\eta^2 - 8K\eta^4\right) \left(\frac{\partial f}{\partial \eta}\right)^2 + \left(6\eta^2 - M^2 + 36Kf\eta^4 - 2f\eta\right) \frac{\partial f}{\partial \eta} + \eta^4 \frac{\partial^3 f}{\partial \eta^3}, \\ & + \left(6\eta^3 - f\eta^2 + 36Kf\eta^4\right) \frac{\partial^2 f}{\partial \eta^2} - 8K\eta^5 \frac{\partial f}{\partial \eta} \frac{\partial^2 f}{\partial \eta^2} + K\eta^6 \left(\frac{\partial^2 f}{\partial \eta^2}\right)^2, \\ & -2K\eta^6 \frac{\partial f}{\partial \eta} \frac{\partial^3 f}{\partial \eta^3} + 12K\eta^5 f \frac{\partial^3 f}{\partial \eta^3} + K\eta^6 f \frac{\partial^4 f}{\partial \eta^4}. \end{aligned} \tag{30}$$

The boundary conditions (9) in terms of η can be rewritten as

$$f_\eta = 0, \qquad f_{\eta\eta} = 0 \qquad \text{at} \qquad \eta = 0, \tag{31}$$

$$f = 0, \qquad f_\eta = -\sin\tau, \qquad \text{at} \qquad \eta = 1. \tag{32}$$

Because the equation (30) is a differential equation, we can discretise it for L uniformly distributed discrete points in $\eta = \left(\eta_1, \eta_2, \eta_3 \ldots\ldots\ldots \eta_{\{L\}}\right) \in (0, 1)$ with a space grid size of $\Delta\eta = 1/(L+1)$ and the time levels $t = (t^1, t^2, \ldots\ldots\ldots)$. Hence the discrete values $(f_1^n, f_2^n, \ldots\ldots\ldots f_L^n)$ at these grid points for the time step $t^n = n\Delta t$ (Δt is the time step size) can be numerically solved together with the boundary conditions at $\eta = \eta_0 = 0$ and $\eta = \eta_{\{L+1\}} = 1$, (31) and (32), as the initial conditions are given. We start our simulations from a motionless velocity field as

$$f\left(\eta, \tau = 0\right) = 0.$$

We will see that a periodic motion will be immediately reached within the first period. We construct a semi-implicit time difference for f and assure that only linear equations for the new time step $(n+1)$ need to be solved

$$\begin{aligned} & S\left(1 - 6K\eta^2\right) \frac{1}{\Delta t} \left(\frac{\partial f^{(n+1)}}{\partial \eta} - \frac{\partial f^{(n)}}{\partial \eta}\right) - SK\eta^4 \frac{1}{\Delta t} \left(\frac{\partial^3 f^{(n+1)}}{\partial \eta^3} - \frac{\partial^3 f^{(n)}}{\partial \eta^3}\right) \\ & -6SK\eta^3 \frac{1}{\Delta t} \left(\frac{\partial^2 f^{(n+1)}}{\partial \eta^2} - \frac{\partial^2 f^{(n)}}{\partial \eta^2}\right) \\ = \; & \left(\eta^2 - 8K\eta^4\right) \left(\frac{\partial f^{(n)}}{\partial \eta}\right)^2 + \left(6\eta^2 - M^2\right) \frac{\partial f^{(n+1)}}{\partial \eta} + \left(36K\eta^4 - 2\eta\right) f^{(n)} \frac{\partial f^{(n)}}{\partial \eta} + 6\eta^3 \frac{\partial^2 f^{(n+1)}}{\partial \eta^2} \\ & + \left(36K\eta^4 - \eta^2\right) f^{(n)} \frac{\partial^2 f^{(n)}}{\partial \eta^2} - 8K\eta^5 \frac{\partial f^{(n)}}{\partial \eta} \frac{\partial^2 f^{(n)}}{\partial \eta^2} + K\eta^6 \left(\frac{\partial^2 f^{(n)}}{\partial \eta^2}\right)^2 + \eta^4 \frac{\partial^3 f^{(n+1)}}{\partial \eta^3}, \\ & -2K\eta^6 \frac{\partial f^{(n)}}{\partial \eta} \frac{\partial^3 f^{(n)}}{\partial \eta^3} + 12K\eta^5 f^{(n)} \frac{\partial^3 f^{(n)}}{\partial \eta^3} + K\eta^6 f^{(n)} \frac{\partial^4 f^{(n)}}{\partial \eta^4}. \end{aligned} \tag{33}$$

It should be noted that other different time differences are also possible. By means of the finite-difference method we can obtain a linear equation system for each time step, which can be solved e.g. by Gaussian elimination.

5 Results and discussion

We compute the velocity field by solving Eq. (8) with the boundary conditions (9) both analytically and numerically. To obtain the analytic series solutions we have used the new analytic technique, namely, the homotopy analysis method (HAM). For the numerical solution, first we solve the initial boundary-value problem in the computational space $\eta \in [0, 1]$ and then the numerical solutions are transformed to the physical space with y-coordinate $y \in [0, \infty)$. The velocity field f' $(= f_y)$ is plotted to observe the influence of the various involving parameters, for example, the viscoelastic parameter K, the Hartman number or magnetic parameter M and the non-dimensional relative amplitude of frequency to the stretching rate S for the time series of the first five periods $\tau \in [0, 10\pi]$ and the transverse profiles. Furthermore, we calculate and show the values of the skin-friction coefficient $\mathrm{Re}_x^{1/2} C_f$ both graphically and in tabular form.

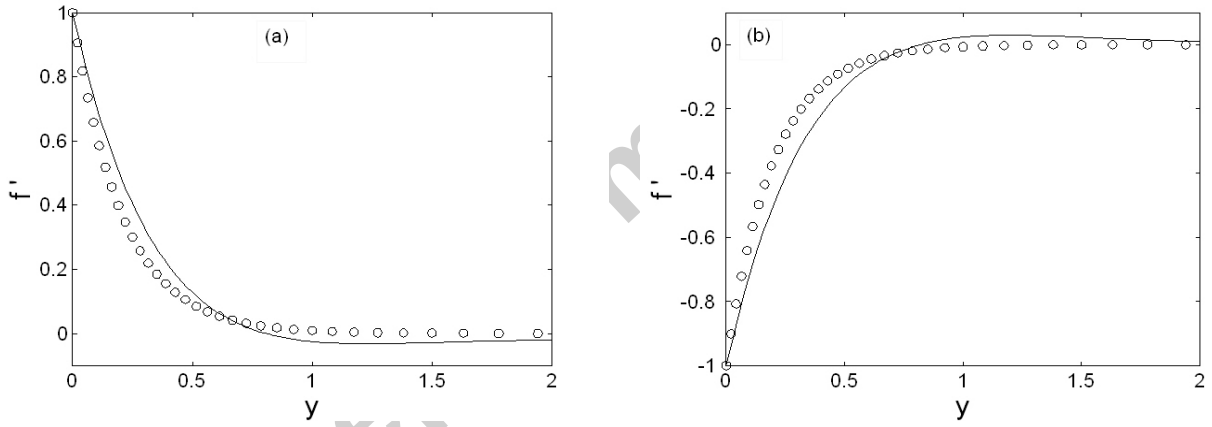

Fig. 3. Comparison of $f'(y, \tau)$ obtained from the HAM solution at the 5th-order of approximation (solid lines) and the numerical solution (open circles) with $S = 1$, $M = 5$ and $K = 0.1$ for two different times (a) $\tau = 0.5\pi$ and (b) $\tau = 1.5\pi$, respectively.

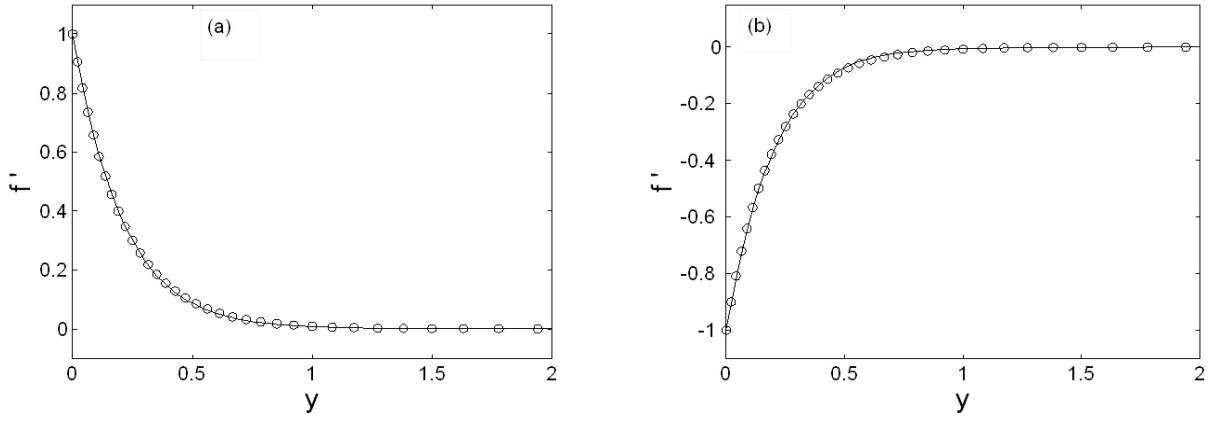

Fig. 4. Comparison of $f'(y, \tau)$ obtained from the HAM solution at the 25th-order of approximation (solid lines) and the numerical solution (open circles) with $S = 1$, $M = 5$ and

$K = 0.1$ for two different times (a) $\tau = 0.5\pi$ and (b) $\tau = 1.5\pi$, respectively.

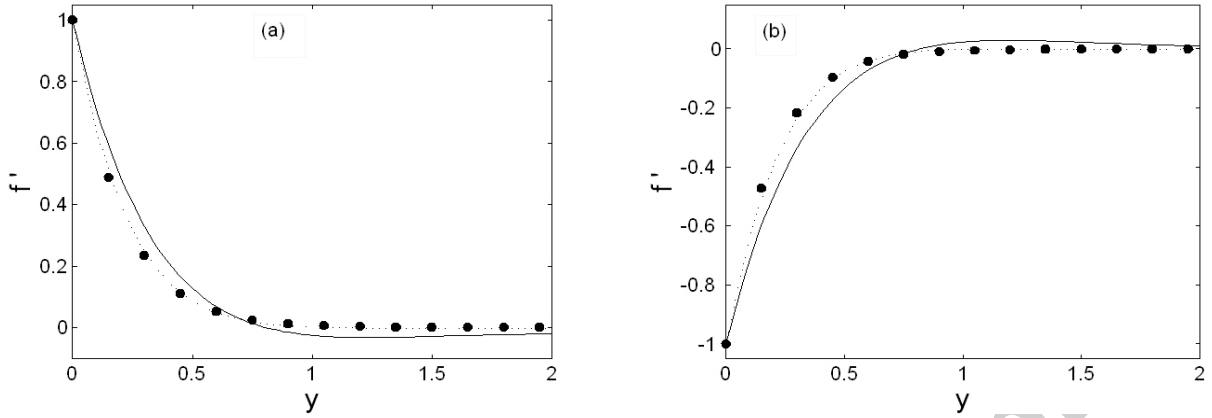

Fig. 5. Approximation of $f'(y, \tau)$ with $S = 1$, $M = 5$ and $K = 0.1$. Solid line: 5th-order approximation; Dashed line: 15th-order approximation; Filled circle: 25th-order approximation for two different times (a) $\tau = 0.5\pi$ and (b) $\tau = 1.5\pi$.

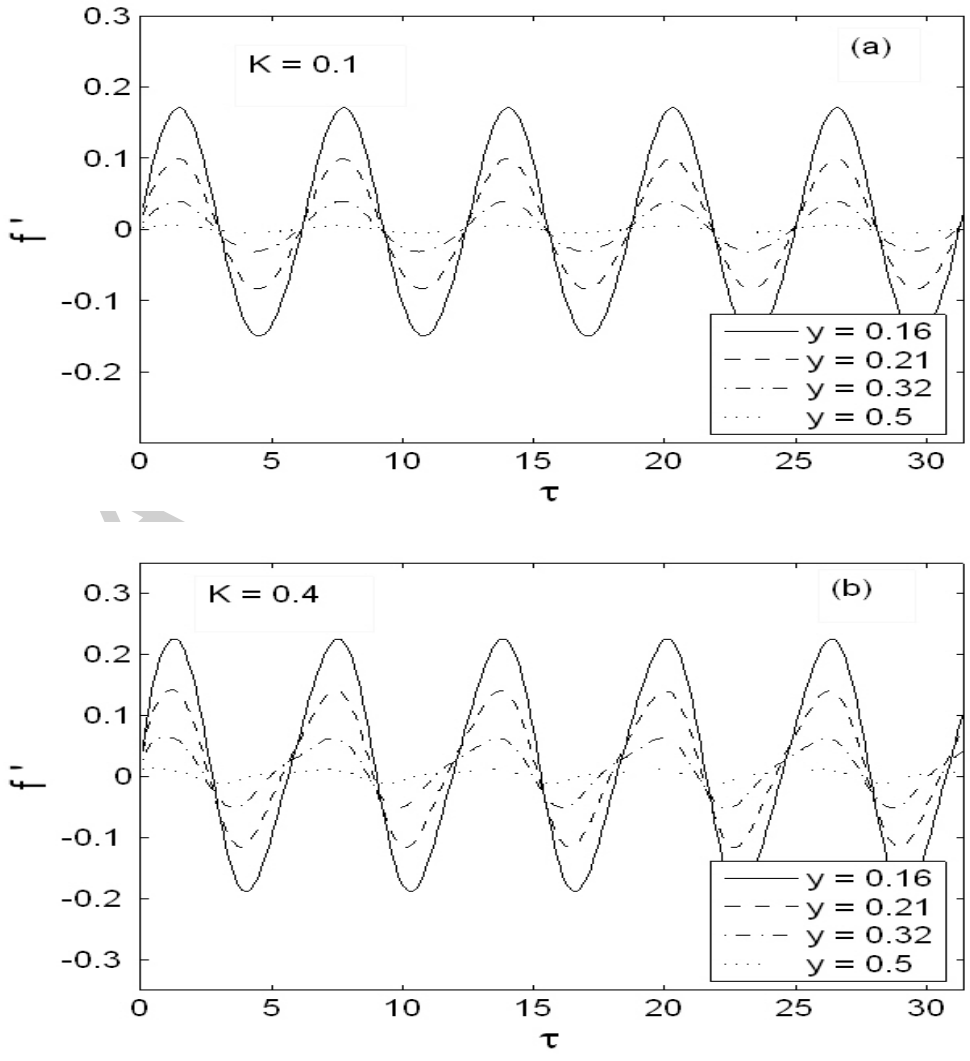

Fig. 6. Time series of the flow of the velocity field f' at the four different distances from the surface for the time period $\tau \in [0, 10\pi]$ with $S = 2$, $M = 10$: (a) $K = 0.1$, (b) $K = 0.4$.

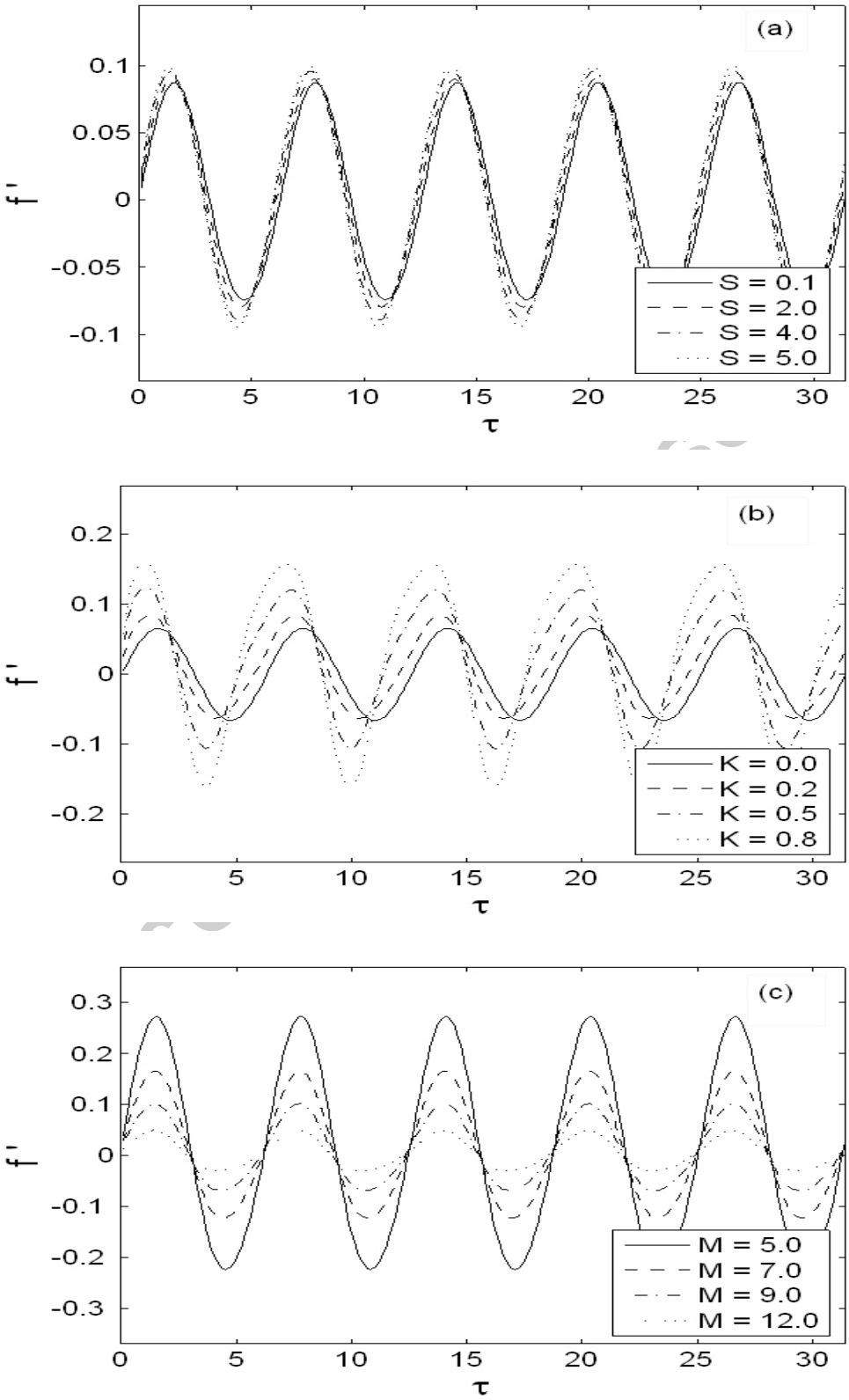

Fig. 7. Time series of the velocity field f' in the first five periods $\tau \in [0, 10\pi]$ at a fixed distance to the sheet, $y = 0.25$: (a) effects of S with $K = 0.2$, $M = 10$, (b) effects of

viscoelastic parameter K with $S = 2$, $M = 10$ and (c) effects of the magnetic parameter M with $S = 1$, $K = 0.2$.

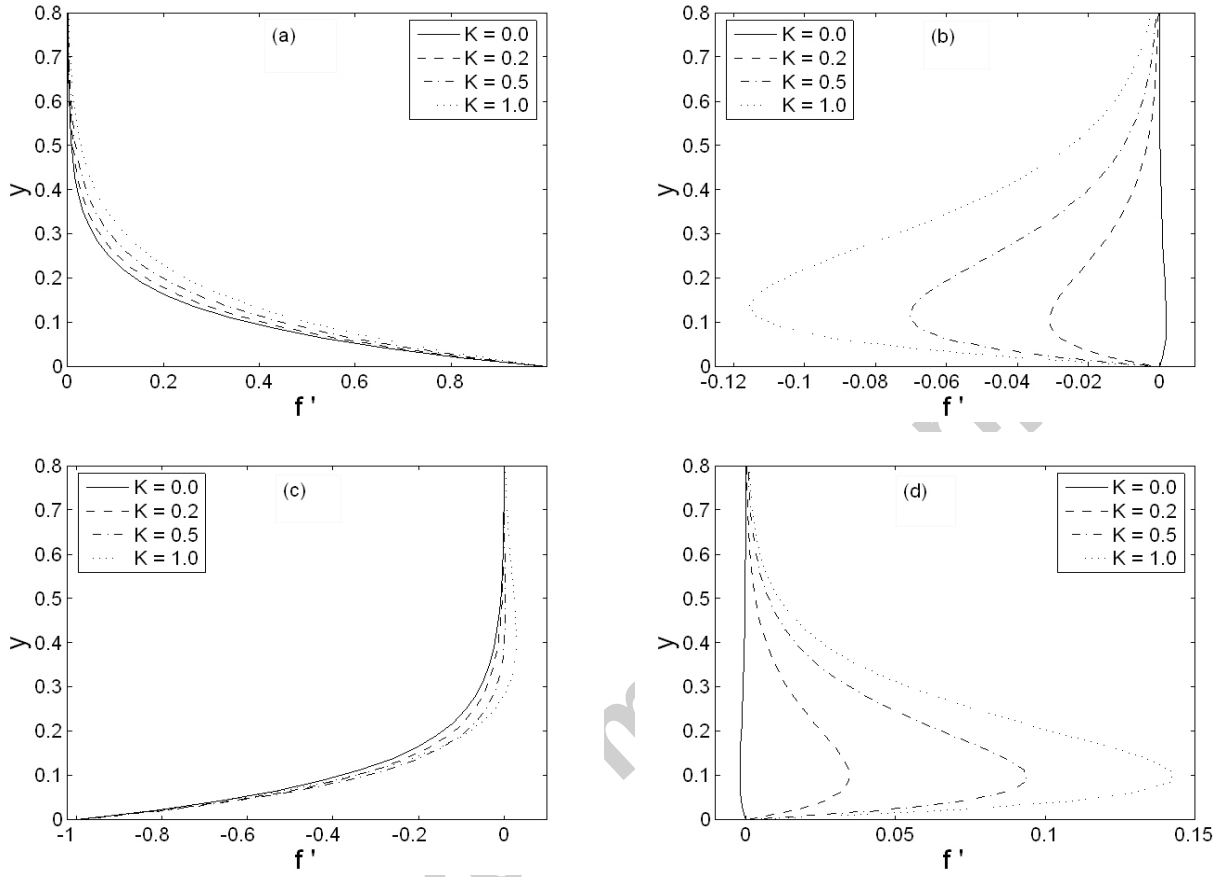

Fig. 8. Transverse profiles of the velocity field f' at the four different values of K for the fifth period $\tau \in [8\pi, 10\pi]$ for which a periodic velocity field has been reached: (a) $\tau = 8.5\pi$, (b) $\tau = 9\pi$, (c) $\tau = 9.5\pi$ and (d) $\tau = 10\pi$ with $S = 2$ and $M = 10$.

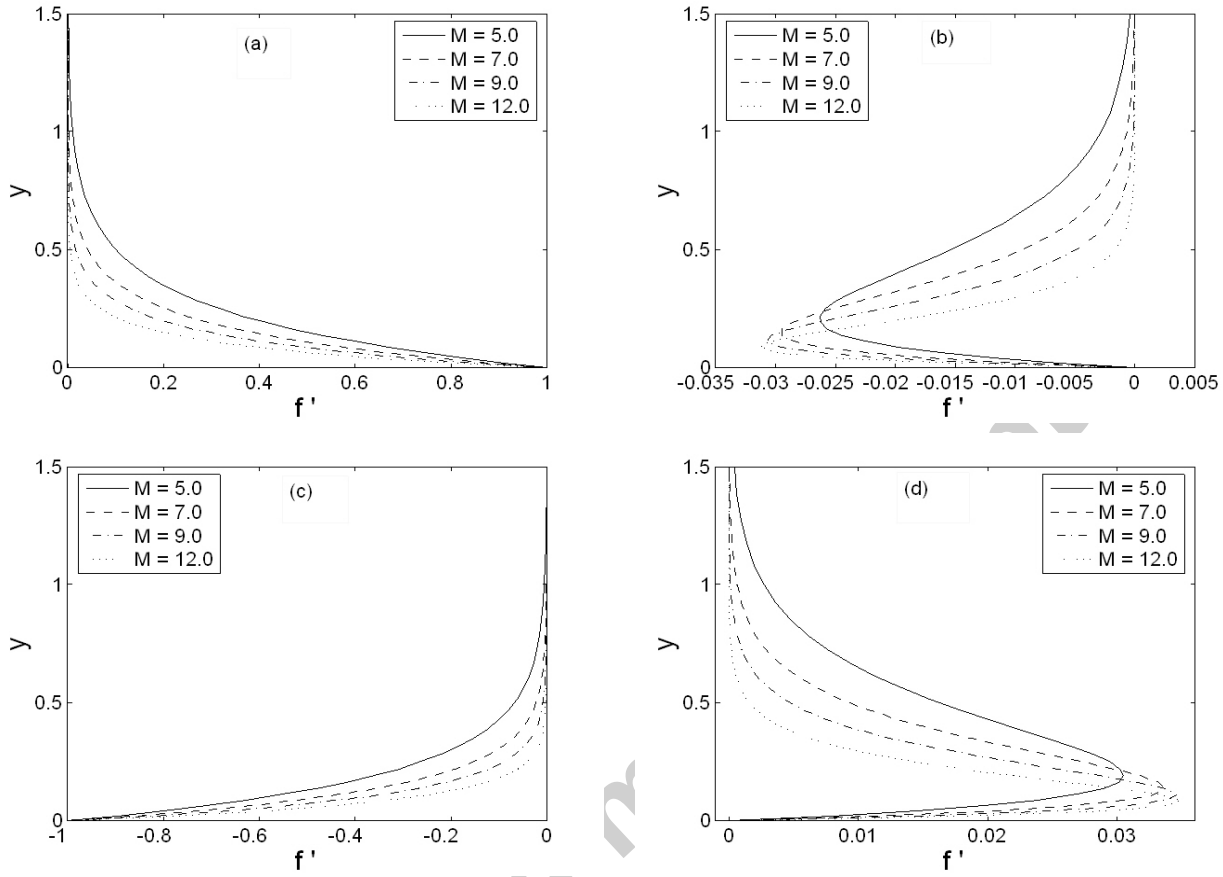

Fig. 9. Transverse profiles of the velocity field f' at the four different values of M for the fifth period $\tau \in [8\pi, 10\pi]$ for which a periodic velocity field has been reached: (a) $\tau = 8.5\pi$, (b) $\tau = 9\pi$, (c) $\tau = 9.5\pi$ and (d) $\tau = 10\pi$ with $S = 1$ and $K = 0.2$.

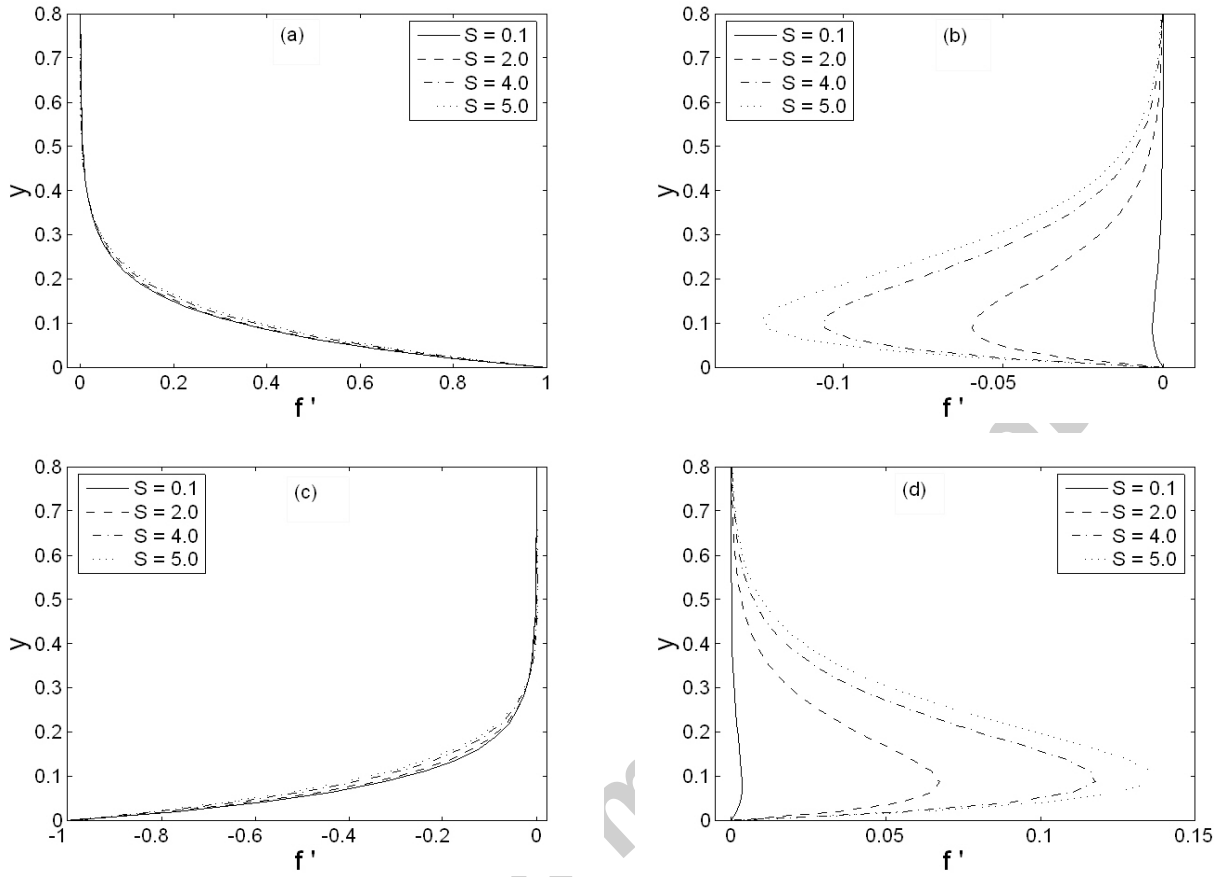

Fig. 10. Transverse profiles of the velocity field f' at the four different values of S for the fifth period $\tau \in [8\pi, 10\pi]$ for which a periodic velocity field has been reached: (a) $\tau = 8.5\pi$, (b) $\tau = 9\pi$, (c) $\tau = 9.5\pi$ and (d) $\tau = 10\pi$ with $K = 0.2$ and $M = 12$.

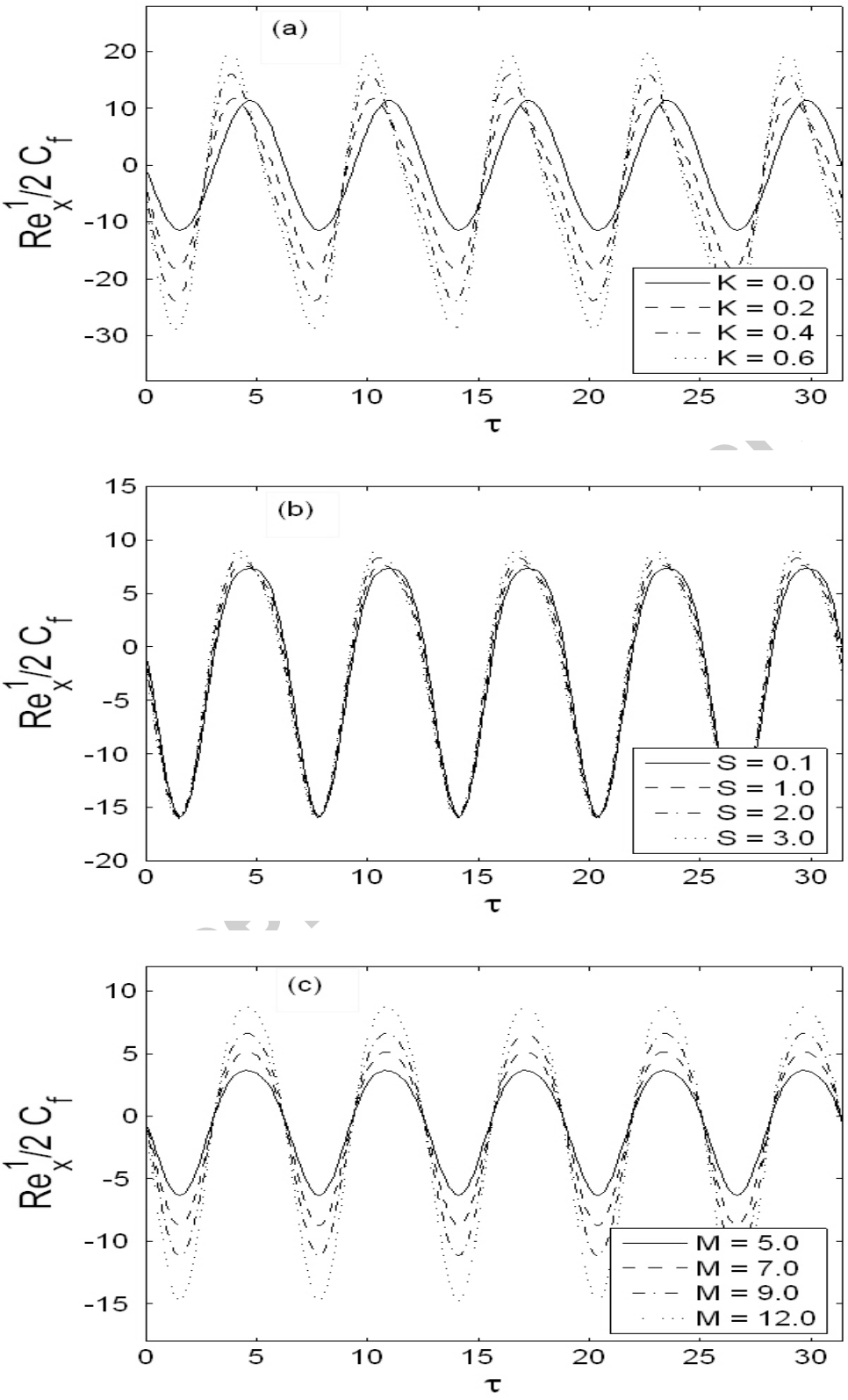

Fig. 11. Time series of the skin-friction coefficient $\mathrm{Re}_x^{1/2} C_f$ in the first five periods $\tau \in [0, 10\pi]$: (a) effects of K with $S = 5$, $M = 12$, (b) effects of S with $K = 0.1$, $M = 12$ and (c) effects of M with $K = 0.1$, $S = 1$.

K	S	M	$\tau = 1.5\pi$	$\tau = 5.5\pi$	$\tau = 9.5\pi$
0.0	1.0	12.0	11.678656	11.678707	11.678656
0.2			5.523296	5.523371	5.523257
0.5			−3.899067	−3.899268	−3.899162
0.8			−11.674383	−11.676506	−11.676116
1.0			−15.617454	−15.624607	−15.624963
0.2	0.5		5.322161	5.322193	5.322173
	1.0		5.523296	5.523371	5.523257
	2.0		6.087060	6.087031	6.087156
	3.0		6.769261	6.768992	6.769294
	4.0		7.497932	7.496924	7.496870
	5.0		8.232954	8.229085	8.228996
	1.0	5.0	2.323502	2.323551	2.323548
		7.0	3.278018	3.278005	3.278123
		9.0	4.197624	4.197771	4.197733
		12.0	5.523296	5.523371	5.523257
		15.0	6.791323	6.791301	6.791278

Table 2. Values of the skin-friction coefficient $\mathrm{Re}_x^{1/2} C_f$ for different values of K, S and M for three different time points $\tau = 1.5\pi$, 5.5π and 9.5π.

For the HAM solution, the higher the order of approximation is, the more accurate is the HAM solution. If the HAM solution does nearly not change any longer with the increase of the order of approximation, the HAM analytical solution can be considered as the exact solution. For the problem investigated it is the case with the 20th-order of approximation (see Table 1). We can also obtain the accuracy/error of the HAM solution by comparing the HAM solution with the convergent numerical solution as displayed in Figs. 3 and 4

Figs. 3-5 are depicted just to compare the homotopy analysis solution and the numerical solution with fixed $S = 1$, $M = 5$, $K = 0.1$ and two different times $\tau = 0.5\pi$ and $\tau = 1.5\pi$. Figs. 3 and 4 show the comparison between the HAM solutions with the 5th and 25th-order of approximation and the numerical solution, respectively. The results show that the HAM solution with the 5th-order of approximation is obviously deviated from the numerical solution, as displayed in Fig. 3. As the order of approximation of the HAM solution is increased, the excellent agreement of HAM solution to the numerical solution for both at $\tau = 0.5\pi$ and $\tau = 1.5\pi$ is demonstrated, as we can see from Fig. 4 by comparing the HAM solution with the 25th-order approximation with the numerical solution. Fig. 5 gives the comparison of the velocity field f' of the HAM solutions with three different orders of approximation at $\tau = 0.5\pi$ and $\tau = 1.5\pi$. It is also observed that the analytic solution obtained by the homotopy analysis method has good agreement for higher order of approximation, for example, with 15th and 25th-orders of approximation, whilst the HAM solution with the 5th-order of approximation has a visible deviation from the higher-order solutions. Obviously, the higher order of approximation the HAM solution has, the closer to the exact solution is the analytic solution.

In the following discussions we will present only numerical solutions. Fig. 6 shows the time series of the velocity field f' at the four different distances from the oscillatory sheet for the first five periods $\tau \in [0, 10\pi]$ with fixed values of $S = 2$, $M = 10$ and $K = 0.1$, 0.4, respectively. It can be seen from Fig. 6(a) ($K = 0.1$) that the amplitude of the flow near the

oscillatory surface is larger as compared to that far away from the surface. As the distance increases from the surface, the amplitude of the flow motion is decreased and almost vanishes (approached to zero) for larger distance from the sheet. From Fig. 6(b), we observe the similar phenomenon for the value of $K = 0.4$. However, for $K = 0.4$ the amplitude of the flow motion is larger as compared with the analysis at $K = 0.1$. That indicates as increased effective viscosity with the increase of the non-Newtonian parameter K.

Fig. 7 illustrates the effects of the non-dimensional relative amplitude of frequency to the stretching rate S, the viscoelastic parameter K and the magnetic parameter M on the time series of the velocity field f' at a fixed distance $y = 0.25$ from the surface, respectively. Fig. 7(a) shows that with the increase of S the amplitude of the flow increases slightly and a phase shift occurs which increases with the increase of S. The influence of the viscoelastic parameter K on the time series of the velocity f' can be seen from Fig. 7(b) with fixed values of $S = 2$ and $M = 10$. We see that the amplitude of the flow motion is increased by increasing the viscoelastic parameter K due to the increased effective viscosity. Similarly to the effects of S, a phase difference occurs for different values of K. Fig. 7(c) shows the time series of the velocity profile f' for the different values of the magnetic parameter M with fixed values of $S = 1$ and $K = 0.2$. As expected, the amplitude of the flow decreases with the increase of the magnetic parameter M. This is because for the investigated problem the magnetic force acts as a resistance to the flow. Only slight phase difference occurs among the time series for different values of M in comparison with those for different values of S and K.

Fig. 8 gives the effects of the viscoelastic parameter K on the transverse profiles of the velocity f' for the different times of $\tau = 8.5\pi, 9\pi, 9.5\pi$ and 10π in the fifth period $\tau \in [8\pi, 10\pi]$ for which a periodic motion has been reached. Fig. 8(a) shows that at $\tau = 8.5\pi$, $f' = 1$ at the surface $y = 0$ equating the sheet velocity and $f' \to 0$ far away from the sheet. It can also be seen that at this point of time, there is no oscillation in the velocity profile and the velocity field f' is increased as the values of K increases, i.e. the boundary layer becomes thickener with the increase of K. Fig. 8(b) gives the velocity profile f' at time point $\tau = 9\pi$. At this time point the velocity field f' is zero at the surface $y = 0$ and far away from the wall it again approaches to zero. It is also evident that near the wall, there exist some oscillation in the velocity profile and the amplitude of the flow increases as K increases. This oscillation in the transverse profile is an evidence of a phase shift in the viscoelastic fluid ($K \neq 0$) against the viscous Newtonian fluid ($K = 0$). The velocity profiles for others two time points within the fifth period are displayed in Figs. 8c-d. For the Newtonian fluid, the flow in the whole flow domain is almost in phase with the sheet oscillation, as shown from the solid lines displayed in Figs. 8a-d (for $K = 0$). The boundary layer thickness increases by increasing the viscoelastic parameter K, as we can see from Fig. 8.

Fig. 9 illustrates the influence of the magnetic parameter M on the transverse profiles of the velocity field f' for the different times of $\tau = 8.5\pi, 9\pi, 9.5\pi$ and 10π. It can be seen that the influence of the magnetic field causes to reduce the boundary layer thickness. As expected, the magnetic force is a resistance to the flow, hence reduces the velocity magnitude. Similar effects have also been shown in previous papers of MHD flows, e.g. [46, 47, 48, 49]. Although for $\tau = 9\pi$ (Fig. 9b) and $\tau = 10\pi$ (Fig. 9d), there exist still velocity oscillations in the transverse profiles, their amplitudes are fairly small (in comparison with those in Fig. 8 (b,d)). It means that for different values of M, the phase difference is almost invisible, which is in the agreement to the results shown in Fig. 7(c).

Fig. 10 shows the effects of the non-dimensional relative amplitude of frequency to the stretching rate S on the velocity f' for the different times of $\tau \in [8.5\pi, 9\pi, 9.5\pi, 10\pi]$ in the

fifth period. Fig. 10(a) is plotted for the variations of S on the velocity f' at time $\tau = 8.5\pi$ at the surface. It is noted that the velocity is equal to the sheet velocity $f' = 1$ at the surface $y = 0$ and far away from the wall it is zero. The velocity f' increases only slightly with the increase of S. Fig. 10(b) shows the influence of S on the velocity f' at time $\tau = 9\pi$. It can be seen that for very small values of $S = 0.1$ at this time point, the velocity in the whole transverse section takes its value at the plate almost to zero ($f' \to 0$), i.e., for small values of S no phase difference occurs with the increase of the distance from the plate and the flow in the whole flow domain is in phase with the sheet motion. However, with the increase of S, a phase difference occurs and increases, as shown also in Fig. 7(a). The velocity profiles for others two time points within the fifth period are plotted in Figs. 10c-d and the similar observations are found as in Figs. 10a-b, respectively.

Fig. 11 gives the variations of the viscoelastic parameter K, the relative amplitude of frequency to the stretching rate and the magnetic parameter M on the skin friction coefficient $\mathrm{Re}_x^{1/2} C_f$ for the time series in the first five periods $\tau \in [0, 10\pi]$. Fig. 11(a) illustrates the influence of the viscoelastic parameter K on the skin friction coefficient $\mathrm{Re}_x^{1/2} C_f$ with fixed $S = 5$ and $M = 12$. It is noted that the skin friction coefficient varies also periodically due to the oscillatory surface motion. The oscillation amplitude of skin friction coefficient $\mathrm{Re}_x^{1/2} C_f$ increases as the values of K are increased. Fig. 11(b) shows the effects of S on the skin friction coefficient $\mathrm{Re}_x^{1/2} C_f$. It can be seen that the oscillation amplitude of the skin friction coefficient increases as S increases. Fig. 11(c) displays the results of the magnetic number M on the skin friction coefficient $\mathrm{Re}_x^{1/2} C_f$ with fixed $S = 1$ and $K = 0.1$. It is observed that the oscillation amplitude of the skin friction coefficient $\mathrm{Re}_x^{1/2} C_f$ is increased by increasing the values of M.

Table 2 shows the numerical values of the skin friction coefficient $\mathrm{Re}_x^{1/2} C_f$ for different values of K, S and M at the different periods of time series. The results show that the values of the skin friction coefficient for the three different time points $\tau = 1.5\pi, 5.5\pi$ and 9.5π are almost identical. It means that the periodic motion may be reached within the first period when the initial conditions are set up. The change of the skin friction coefficient from positive to negative with the increase of K indicates the large phase difference with the increase of K, as shown in Fig. 11(a) (but for slightly different parameters). It can also be seen that the values of the skin friction coefficient $\mathrm{Re}_x^{1/2} C_f$ are increased as the relative frequency to the stretching rate S or/and the magnetic field M are increased. A change in the sign of skin-friction does not appear for different values of S and M cause mainly the change on the values of the skin-friction, less on the phase difference.

6 Concluding remarks

In the present investigation, the boundary layer flow of the MHD viscoelastic fluid over an oscillatory stretching sheet has been discussed. The obtained flow equation is solved both analytically using homotopy analysis method and numerically by means of the finite difference method. The comparison between both solutions is given and found in excellent agreement for the HAM solution with higher-order approximation. It demonstrates the convergence of the presented HAM solution for the investigated problem. The influence of the different parameters on the transverse profiles and the time series of velocity is illustrated and discussed. The numerical results give a view towards understanding the response characteristics of the second grade viscoelastic fluid.

Acknowledgment: The authors are grateful to the referee for his/her useful comments. One of the authors Z. Abbas gratefully acknowledges the financial support provided for this study by the Higher Education Commission (HEC) Pakistan under the International Research Support Initiative Program (IRSIP).

References

[1] K. R. Rajagopal, On boundary conditions for fluids of the differential type, in:A Sequira (Ed.), Navier-Stokes equations and related non-linear problems, Plenum, New York, 1995, pp.273-278.

[2] K. R. Rajagopal and P. N. Kaloni, Some remarks on boundary conditions for fluids of the differential type, in: G. A. C. Graham, S. K. Malik (Eds.), Continuum Mechanics and its Applications, Hemisphere, New York, 1989, pp.935-942.

[3] K. R. Rajagopal, On the creeping flow of second order fluid, J. Non-Newtonian Fluid Mech. **15** (1984) 239-246.

[4] K. R. Rajagopal and A. S. Gupta, An exact solution for the flow of a non-Newtonian fluid past an infinite porous plate, Meccanica **19** (1984) 158-160.

[5] A. Z. Szeri and K. R. Rajagopal, Flow of a non-Newtonian fluid between heated parallel plates, Int. J. Nonlinear Mech. **20** (1985) 91-101.

[6] W. C. Tan and T. Masuoka, Stokes'first problem for a second grade fluid in a porous half-space with heated boundary, Int. J. Non-Linear Mech. **40**, 515-522 (2005).

[7] W. Tan and T. Masuoka, Stokes'first problem for an Oldroyd-B fluid in a porous half-space, Phys. fluids **17**, 023101-7 (2005).

[8] C. Fetecau and C. Fetecau, On some axial Couette flows of a non-Newtonian fluid, Z. Angew. Math. Phys. **56** (2005) $1098 - 1106$.

[9] C. Fetecau and C. Fetecau, Starting solutions for the motion of a second grade fluid due to longitudinal and torsional oscillations of a circular cylinder, Int. J. Eng. Sci. **44** (2006) $788 - 796$.

[10] C. Fetecau and C. Fetecau, Decay of a potential vortex in an Oldroyd-B fluid, Int. J. Eng. Sci. **43** (2005) $430 - 351$.

[11] T. Hayat and A. H. Kara, Couette flow of a third grade fluid with variable magnetic field, Math. Computer Modelling **43** (2006) $132 - 137$.

[12] M. Khan, T. Hayat and S. Asghar, Exact solution for MHD flow of a generalized Oldroyd-B fluid with modified Darcy's law, Int. J. Eng. Sci. **44** (2006) $333 - 339$.

[13] T. Hayat, Z. Abbas, M. Sajid and S. Asghar, The influence of thermal radiation on MHD flow of a second grade fluid, Int. J. Heat Mass Transfer **50** (2007) $931 - 941$.

[14] T. Hayat, S. B. Khan and M. Khan, The influence of Hall current on the rotating oscillating flows of an Oldroyd-B fluid in a porous medium, Non-Linear Dyn. **47** (2007) $353-362$.

[15] T. Hayat, Z. Abbas and M. Sajid, On the analytic solution of MHD flow of a second grade fluid over a shrinking sheet, ASME J. Appl. Mech. **74** (2007) 1165 − 1171.

[16] T. Hayat, T. Javed and M. Sajid, Analytical solution for rotating flow and heat transfer analysis of a third-grade fluid, Acta Mech. **191** (2007) 219 − 229.

[17] 14. R. Cortell, Toward an understanding of the motion and mass transfer with chemically reactive species for two classes of viscoelastic fluid over a porous stretching sheet, Chem.Eng. Processing **46** (2007) 982-989.

[18] B.C.Sakiadis, Boundary layer behavior on continuous solid surfaces, Am.Inst.Chem.Eng.J. **7** (1961) 26-28.

[19] K. R. Rajagopal, T. Y. Na and A. S. Gupta, Flow of a viscoelastic fluid over a stretching sheet, Rheol. Acta, **23** (1984)213-215.

[20] R. Cortell, Viscoelastic fluid flow and heat transfer over a stretching sheet under the effects of a non-uniform heat source, viscous dissipation and thermal radiation, Int.J.Heat and Mass Transfer **50** (2007) 3152-3162.

[21] R. Cortell, Effects of viscous dissipation and work done by deformation on the MHD flow and heat transfer of a viscoelastic fluid over a stretching sheet, Phys. Lett. A **357** (2006)298-305.

[22] P. D. Ariel, T. Hayat and S. Asghar, Homotopy perturbation method and axisymmetric flow over a stretching sheet, Int. J. Non-linear Sci. Numer. Simulation **7** (2006) 399-406.

[23] M. Sajid, T. Hayat and S. Asghar, Non-similar solution for the axisymmetric flow of a third grade fluid over a radially stretching sheet, Acta Mech. **189** (2007) 193-205.

[24] C. Y. Wang, Nonlinear streaming due to the oscillatory stretching of a sheet in a viscous fluid, Acta Mech. **72** (1988) 261-268.

[25] V. M. Soundalgekar and S. K. Gupta, Free convection effects on the oscillatory flow of a viscous, incompressible fluid past a steadily moving vertical plate with constant suction, Int. J. Heat Mass Transfer **18** (1975) 1083–1093.

[26] A. K. Khaled and K. Vafai, Analysis of flow and heat transfer inside oscillatory squeezed thin films subject to a varying clearance, Int. J. Heat Mass Transfer **46** (2003) 631-641.

[27] S. J. Liao, Beyond perturbation: introduction to homotopy analysis method, Boca Raton: Chapman & Hall/CRC Press; 2003.

[28] S. J. Liao, Application of process analysis method to the solution of 2D nonlinear progressive gravity waves, J. Ship. Res. **36** (1992) 30 − 37.

[29] S. J. Liao, An analytic solution of unsteady boundary-layer flows caused by an impulsively stretching plate, Comm. Non-linear Sci. Numer. Simm. **11** (2006) 326 − 339.

[30] Y. Tan and S. J . Liao, Series solution of three-dimensional unsteady laminar viscous flow due to a stretching surface in a rotating fluid, ASME J. Appl. Mech. **74** (2007) 1011-1018.

[31] H. Xu and S. J. Liao, Series solution of unsteady magnetohydrodynamic flows of non-Newtonian fluids caused by an impulsively stretching plate, J. Non-Newtonian Fluid Mech. **129** (2005) 46-55.

[32] S. J. Liao, A new branch of solutions of boundary-layer flows over a permeable stretching plate, Int. J. Non-Linear Mech. **42** (2007) 819 – 830.

[33] L. Zou, Z. Zong, Z. Wang and L. He, Solving the discrete KdV equation with homotopy analysis method, Phys. Lett. A **370** (2007) 287-294.

[34] S. Abbasbandy, The application of homotopy analysis method to nonlinear equations arising in heat transfer, Phys. Lett. A **360** (2006) 109 – 113.

[35] Y. Tan and S. Abbasbandy, Homotopy analysis method for quadratic Recati differential equation, Comm. Non-linear Sci. Numer. Simm. **13** (2008) 539 – 546.

[36] S. Abbasbandy and F.S. Zakaria, Soliton solutions for the fifth-order KdV equation with the homotopy analysis method, Nonlinear Dyn **51** (2008) 83 – 87.

[37] T. Hayat, Z. Abbas and M. Sajid, Series solution for the upper-convected Maxwell fluid over a porous stretching plate, Phys. Lett. A **358** (2006) 396 – 403.

[38] M. Sajid, T. Hayat and S. Asghar, On the analytic solution of steady flow of a fourth grade fluid, Phys. Lett. A **355** (2006) 18 – 24.

[39] Z. Abbas, M. Sajid and T. Hayat, MHD boundary layer flow of an upper-convected Maxwell fluid in porous channel, Theor. Comp. Fluid Dyn. **20** (2006) 229 – 238.

[40] M. Sajid, T. Hayat and S. Asghar, Comparison of the HAM and HPM solutions of thin film flows of non-Newtonian fluids on a moving belt, Nonlinear Dyn. **50** (2007) 27 – 35.

[41] T. Hayat and M. Sajid, On analytic solution for thin film flow of a fourth grade fluid down a vertical cylinder, Phys. Lett. A **361** (2007) 316 – 322.

[42] T. Hayat and Z. Abbas, Heat transfer analysis on the MHD flow of a second grade fluid in a channel with porous medium, Choas Solitons & Fractals (in press).

[43] T. Hayat, Z. Abbas and T. Javed, Mixed convection flow of a micropolar fluid over a non-linearly stretching sheet, Phys. Lett. A (in press).

[44] M. Sajid, T. Hayat and S. Asgher, Non-similar analytic solution for MHD flow and heat transfer in a third-order fluid over a stretching sheet, Int. J. Heat Mass Transfer **50** (2007) 1723-1736.

[45] V. K. Garg and K. R. Rajagopal, Flow of non-Newtonian fluid past a wedge, Acta Mech. **88** (1991) 113 – 123.

[46] R. Cortell, A note on magnetohydrodynamic flow of a power-law fluid over a stretching sheet, Appl. Math. Comp. **168** (2005) 557 – 566.

[47] R. Cortell Bataller, MHD boundary-layer flow and heat transfer of a non-Newtonian power-law fluid past a moving plate with thermal radiation, II Nuovo Cimento **121** (2006) 951 – 964.

[48] Y. Wang, T. Hayat, N. Ali and M. Oberlack, Magnetohydrodynamic peristaltic motion of a sisko fluid in a symmetric or asymmetric channel, Physica A, **387** (2008) 347 – 362.

[49] Y. Wang and W. Wu, Time-dependent magnetohydrodynamic flow induced by non-coaxial rotations of a non-torsionally oscillating porous plate and a third-order fluid at infinity, Math. Comput. Modelling, **46** (2007) 1277 – 1293.